Instrument Science Report WFC3 2009-041

WFC3 : SMOV- Alternative Geometric Distortion Method

B.M^{c}Lean, C.Cox, V.Kozhurina-Platais, L.Petro, L.Dressel, H.Bushouse, E.Sabbi
March 11, 2010

ABSTRACT

This ISR describes another technique that derives the geometric distortion of the WFC3 directly in the spacecraft (V2,V3) reference frame. Initially developed as an independant check of the previously used technique, it verifies that the distortion solutions are consistent. However, it also highlight's a need to ensure that the distortion coefficients stay in sync with the science instrument aperture file geometry used to schedule any given observation in order to use MultiDrizzle.

Introduction

As part of the SMOV calibration efforts, an alternative method of determining the geometric distortion was developed to provide an independant check of the results. This reduction used the same standard astrometric fields and calibration data, however the analysis was performed directly in the spacecraft (V2,V3) reference frame with the intention of 'stacking' multiple observations to increase the sampling across the instrument field of view. This technique shall be referred to as the (V2,V3) method to distinguish it from the (X,Y) method described in Kozhurina-Platais et al (2009a, 2009b) which does the calibration in a catalog reference frame.

As described in these ISR's, multiple observations of astrometric fields in 47 Tuc and the LMC were observed with the WFC3 in both the UVIS and IR channels in order to map the geometric distortions of the instrument. Astrometric reference stars are identified in each of these images and measured pixel coordinates are directly mapped to predicted (V2,V3) positions using a polynomial distortion model. In the case of the UVIS channel,

we solve the distortion for the 2 chips completely independantly without a requirement to tie the 2 chips together into a single 'metachip'.

Data

The calibration programs used were implemented in proposals 11444 (UVIS Plate Scale) and 11445 (IR Plate Scale) and the images obtained are summarised in Table 1.

Table 1. List of observations used

PropID	Detector	Filter	ExpStart	ExpTime	IPPPSSOOT	Target	RA_aper	Dec_aper	PosTarg1	PosTarg2
1444	UVIS	F606W	55027.51408	350	iabj01yuq	NGC104	5.6631598	-72.0635986	-11	11
11444	UVIS	F606W	55027.51961	350	iabj01yvq	NGC104	5.6467099	-72.0669022	11	11
11444	UVIS	F606W	55027.55195	350	iabj01yxq	NGC104	5.6576700	-72.0719986	11	-11
11444	UVIS	F606W	55027.55748	350	iabj01yzq	NGC104	5.6741300	-72.0686035	-11	-11
11444	UVIS	F606W	55027.56302	350	iabj01z1q	NGC104	5.6905799	-72.0652008	-32.9	-11
11444	UVIS	F606W	55027.56855	350	iabj01z3q	NGC104	5.6796198	-72.0602036	-32.9	11
11444	UVIS	F606W	55027.57408	350	iabj01z5q	NGC104	5.6686602	-72.0550995	-32.9	32.9
11444	UVIS	F606W	55027.57961	350	iabj01z7q	NGC104	5.6522102	-72.0585022	-11	32.9
11444	UVIS	F606W	55027.58515	350	iabj01z9q	NGC104	5.6357498	-72.0618973	11	32.9
11444	UVIS	F606W	55027.62437	350	iabj01zbq	NGC104	5.6192899	-72.0652008	32.9	32.9
11444	UVIS	F606W	55027.62990	350	iabj01zdq	NGC104	5.6302400	-72.0702972	32.9	11
11444	UVIS	F606W	55027.63544	350	iabj01zfq	NGC104	5.6412001	-72.0754013	32.9	-11
11444	UVIS	F606W	55027.64097	350	iabj01zhq	NGC104	5.6521702	-72.0803986	32.9	-32.9
11444	UVIS	F606W	55027.64650	350	iabj01zjq	NGC104	5.6686401	-72.0771027	11	-32.9
11444	UVIS	F606W	55027.65203	350	iabj01zlq	NGC104	5.6851001	-72.0737000	-11	-32.9
11444	UVIS	F606W	55027.67170	350	iabj01znq	NGC104	5.7015600	-72.0702972	-32.9	-32.9
11444	UVIS	F606W	55027.69472	350	iabj01zpq	NGC104	5.6641202	-72.0680008	-3	-3
11444	UVIS	F606W	55027.70025	350	iabj01zrq	NGC104	5.6611600	-72.066597	-3	3
11444	UVIS	F606W	55027.70578	350	iabj01ztq	NGC104	5.6567101	-72.0675964	3	3
11444	UVIS	F606W	55027.71132	350	iabj01zvq	NGC104	5.6596699	-72.0689011	3	-3
11444	UVIS	F606W	55027.71685	350	iabj01zxq	NGC104	5.6614199	-72.0678024	-0.8	-0.8
11444	UVIS	F606W	55027.73806	350	iabj01zzq	NGC104	5.6606202	-72.0674973	-0.8	0.8
11444	UVIS	F606W	55027.76452	350	iabj01a2q	NGC104	5.6594200	-72.0677032	0.8	0.8
11444	UVIS	F606W	55027.77005	350	iabj01a4q	NGC104	5.6602201	-72.0681000	0.8	-0.8
11444	UVIS	F606W	55027.80130	349	iabj02a6q	LMC-FIELD	80.4816971	-69.4990997	0	11
11444	UVIS	F606W	55027.80682	349	iabj02a7q	LMC-FIELD	80.4987030	-69.4977036	0	-11

11444	UVIS	F606W	55027.81234	349	iabj02a9q	LMC-FIELD	80.5031967	-69.4910965	-21.9	-21.9
11444	UVIS	F606W	55027.83443	349	iabj02abq	LMC-FIELD	80.4692993	-69.4937973	-21.9	21.9
11444	UVIS	F606W	55027.86538	349	iabj02adq	LMC-FIELD	80.4772034	-69.5056992	21.9	21.9
11444	UVIS	F606W	55027.87090	349	iabj02afq	LMC-FIELD	80.5111008	-69.5028992	21.9	-21.9
11445	IR	F160W	55035.06892	274.2	iabi01u9q	NGC104	5.6647501	-72.0645981	-9.3	8.3
11445	IR	F160W	55035.07234	274.2	iabi01ubq	NGC104	5.6647501	-72.0645981	-9.3	8.3
11445	IR	F160W	55035.07640	274.2	iabi01udq	NGC104	5.6496401	-72.0668030	9.3	8.3
11445	IR	F160W	55035.07982	274.2	iabi01ufq	NGC104	5.6496401	-72.0668030	9.3	8.3
11445	IR	F160W	55035.10780	274.2	iabi01uqq	NGC104	5.6560898	-72.0709991	9.3	-8.3
11445	IR	F160W	55035.11122	274.2	iabi01usq	NGC104	5.6560898	-72.0709991	9.3	-8.3
11445	IR	F160W	55035.11528	274.2	iabi01uwq	NGC104	5.6711998	-72.0687027	-9.3	-8.3
11445	IR	F160W	55035.11869	274.2	iabi01uyq	NGC104	5.6711998	-72.0687027	-9.3	-8.3
11445	IR	F160W	55035.12960	274.2	iabi01v0q	NGC104	5.6711998	-72.0687027	-9.3	-8.3
11445	IR	F160W	55035.13349	274.2	iabi01v2q	NGC104	5.6711402	-72.0687027	-9.2	-8.3
11445	IR	F160W	55035.13737	274.2	iabi01v4q	NGC104	5.6711202	-72.0687027	-9.2	-8.2
11445	IR	F160W	55035.14126	274.2	iabi01v6q	NGC104	5.6711702	-72.0687027	-9.3	-8.2
11445	IR	F160W	55035.15557	274.2	iabi01v8q	NGC104	5.6862898	-72.0664978	-27.8	-8.3
11445	IR	F160W	55035.17439	274.2	iabi01vaq	NGC104	5.6798401	-72.0624008	-27.8	8.3
11445	IR	F160W	55035.17844	274.2	iabi01vcq	NGC104	5.6733899	-72.0581970	-27.8	24.9
11445	IR	F160W	55035.18250	274.2	iabi01veq	NGC104	5.6582999	-72.0604019	-9.3	24.9
11445	IR	F160W	55035.19423	274.2	iabi01vgq	NGC104	5.6431899	-72.0626984	9.3	24.9
11445	IR	F160W	55035.19829	274.2	iabi01viq	NGC104	5.6280899	-72.0649033	27.8	24.9
11445	IR	F160W	55035.20234	274.2	iabi01vkq	NGC104	5.6345401	-72.0690002	27.8	8.3
11445	IR	F160W	55035.20639	274.2	iabi01vmq	NGC104	5.6409798	-72.0731964	27.8	-8.3
11445	IR	F160W	55035.24097	274.2	iabi01vsq	NGC104	5.6474299	-72.0773010	27.8	-24.9
11445	IR	F160W	55035.24504	274.2	iabi01vvq	NGC104	5.6625400	-72.0751038	9.3	-24.9
11445	IR	F160W	55035.24910	274.2	iabi01vxq	NGC104	5.6776500	-72.0728989	-9.3	-24.9
11445	IR	F160W	55035.25316	274.2	iabi01w0q	NGC104	5.6927500	-72.0707016	-27.8	-24.9
11445	IR	F160W	55045.17965	92.9	iabi02mcq	LMC-FIELD	80.4804993	-69.4989014	0	12.4
11445	IR	F160W	55045.18169	92.9	iabi02meq	LMC-FIELD	80.4744034	-69.5071030	27.8	24.9
11445	IR	F160W	55045.18369	92.9	iabi02mfq	LMC-FIELD	80.4937973	-69.5059967	27.8	0
11445	IR	F160W	55045.19310	92.9	iabi02mhq	LMC-FIELD	80.5132980	-69.5048981	27.8	-24.9
11445	IR	F160W	55045.19514	92.9	iabi02mjq	LMC-FIELD	80.4999008	-69.4978027	0	-12.4
11445	IR	F160W	55045.19718	92.9	iabi02mkq	LMC-FIELD	80.5059967	-69.4896011	-27.8	-24.9
11445	IR	F160W	55045.24639	92.9	iabi02mmq	LMC-FIELD	80.4866028	-69.4906998	-27.8	0
11445	IR	F160W	55045.24839	92.9	iabi02mnq	LMC-FIELD	80.4671021	-69.4918976	-27.8	24.9

Data Characteristics

It should be noted that an *extremely rare* command collision occurred whilst the telescope was attempting to execute the POSTARG motion between observations 2 and 3 of proposal 11444. The effect of this was the POSTARG command failing and the planned motion of (-11.8",+11.8") did NOT occur. The header coordinates of all subsequent images in this visit were consequently in error by this amount and required a manual correction before beginning the analysis.

Another important point for the later analysis is that these observations were obtained with the WFC3 SIAF (Science Instrument Aperture File) entries set to the nominal pre-launch estimates of the instrument aperture geometry. The actual aperture locations were determined on-orbit using the results of calibration programs 11442 (WFC3 UVIS to FGS Alignment) and 11443 (WFC3 IR to FGS Alignment) as part of the SMOV calibration program, but at the time of these observations the corrected values had not yet been updated in the HST ground-system.

Finally, these observations were obtained with the WFC3 *'slightly defocused'* rght before a planned move of the HST focus that would result in a nominal focus for both WFC3 and ACS. The defocus was small enough that we expect it will not significantly affect the centroiding measurements of the stellar PSFs.

Analysis

The first step in the analysis is similar to the (X,Y) technique - measure the centroids of all the stars in the image. However, rather than using the IRAF/DAOPHOT/PHOT task to measure positions, an independent IDL procedure that implemented the object detection and 2-D supergaussian centroiding algorithms used in the GSC-II construction (Lasker et al 2008) was employed. In the cases of typically faint stars, where the 2D centroider failed as a result of the image PSF undersampling, the 1D gaussian fit to the marginal distributions was used.

The identification of the reference catalogue stars was an automated 2-step process. The first step uses the nominal WCS astrometry in the header which is typically accurate to better than 1". The images were subdivided into a 5x5 grid of cells. In each cell the 10 brightest image objects were matched to the 10 brightest catalogue objects in that cell with a large tolerance of ~4". This provides a basic pattern match to start an iterative process of improving the astrometry. A third order polynomial was used to provide an astrometric transformation between (x,y) and standard coordinates (ξ,η). Once the solution converged (typically with residuals of <0.1"), all the objects were rematched to the catalogue and an updated solution obtained with typical residuals of <0.02". This now provided a list of catalog IDs and their positions in both (RA,Dec) and (x,y).

The next step in this analysis was to derive the 'actual' pointing of the HST V1 axis as this is the primary reference point for the HST focal plane. This is not available in the image headers but can be derived from the *jitter* files associated with each observation. The values of the keywords RA_AVG, DEC_AVG and ROLL_AVG which are computed from the FGS telemetry, are the best determination of the position and roll at the commanded aperture position specified by keywords APER_V2 and APER_V3. Using spherical trigonometry, one can then compute the (RA,Dec) of the HST V1 axis.

Given this as the tangent point, the predicted (V2,V3) positions of the reference catalog objects are computed as a tangential projection and a rotation by PA_V3. This angle is derived from the star trackers and is extremely precise. This now gives us a set of measurements in the distorted image (x,y), mapped to the undistorted spacecraft focal plane (V2,V3) to use in deriving the distortion polynomial.

Distortion Solution

The distortion polynomials transforming pixel positions (x,y) to the HST (V2,V3) system are expressed as

$$V2 = a00 + a10.(y-y_{ref}) + a11.(x-x_{ref}) + ..a_{ij}.(x-x_{ref})^{j} .(y-y_{ref})^{i-j}$$
$$V3 = b00 + b10.(y-y_{ref}) + b11.(x-x_{ref}) + ..b_{ij}.(x-x_{ref})^{j} .(y-y_{ref})^{i-j}$$

where x_{ref} and y_{ref} are reference pixels at the center of each chip. A 4^{th} order polynomial was adopted for consistency with the (X,Y) technique even though formal error estimates on the coefficients suggest that a 3^{rd} order polynomial may be sufficient to describe the distortion in this reference frame. The polynomial was solved using the standard IDL *regress* procedure in an iterative loop which used sigma-clipping to reject high-residual outliers. This code was tested pre-launch (without the sigma clipping and iteration) using the Zeemax model data, and it successfully rederived the distortion coefficients and aperture geometry that were in place in the HST ground system.

In addition to solving for the distortion coefficients, as a by-product this technique also derives the zero points, i.e. the position of the chip reference pixels in the HST (V2,V3) focal plane. Whilst this is a useful internal check, we should remember that the spacecraft pointing is defined by the GSC-II reference frame which has a formal positional error of 0.25" and the actual focal plane positions are defined by measurements in an special astrometric field which has a much better precision.

In practice, a separate solution was performed for each chip of each observation in addition to solutions combining measurements of all 47 Tuc observations, all LMC observations and finally everything together. This was done in order to perform a number of internal consistency checks. An example of a typical (V2,V3) residual plot is shown in figure 1 for a measurements from a single UVIS exposure. The density of stars on chip 2 is slightly lower than chip 1 due to their locations with respect to the cluster center.

Typical errors for the distortion fit to each chip are 2-3 mas, and no systematic errors were found as a function of chip position or reference star magnitude.

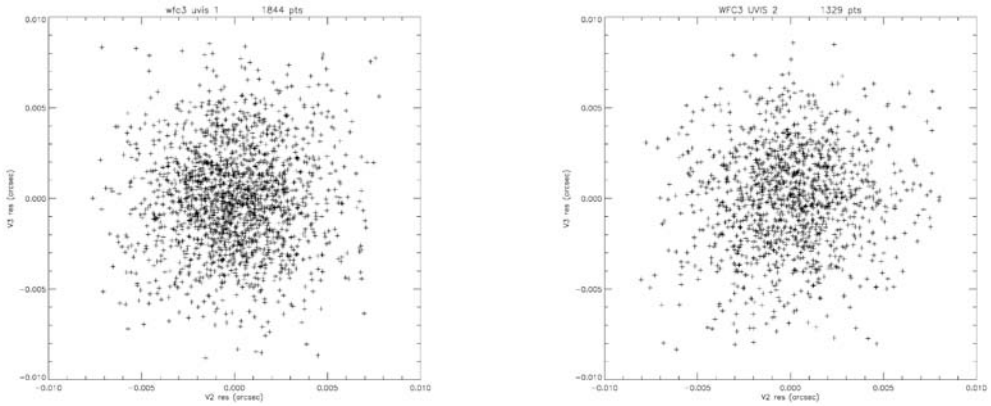

Figure 1 - (V2,V3) residuals between the reference catalog and the distortion solutions for each chip in a typical UVIS exposure in 47 Tuc

As originally conceived, this technique allowed one to 'stack' all measurements together, however if we look at the same residual plot for *all* 47 Tuc exposures shown in figure 2, we find in practice that we see sub-structure or clumping of the residuals from exposure to exposure. In practice, we are seeing the effects of *guider drift* as described by Gilliland (2005) of up to 10-15 mas between exposures.

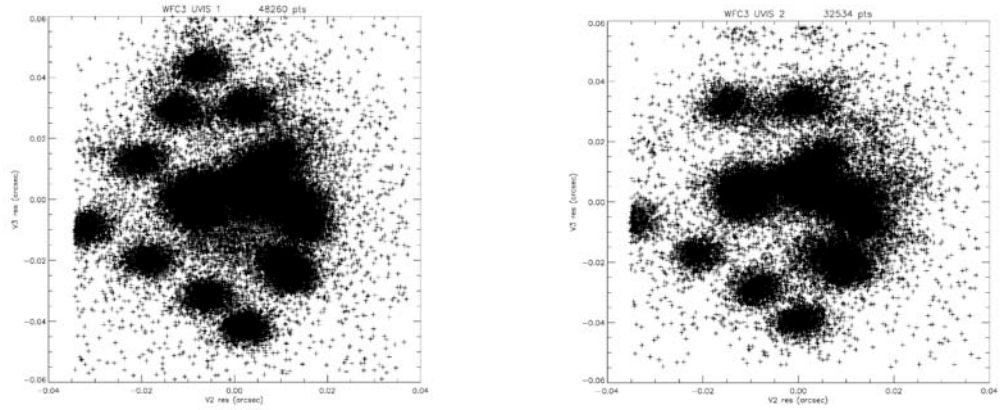

Figure 2 - (V2,V3) residuals between the reference catalog and the combined distortion solutions for all 47 Tuc observations

We collected all the individual distortion solutions into a single Excel spreadsheet for additional analysis, and it is particularly striking that we can see the same clumping in a plot of the V2,V3 zero points for each measurement as shown in figure 3.

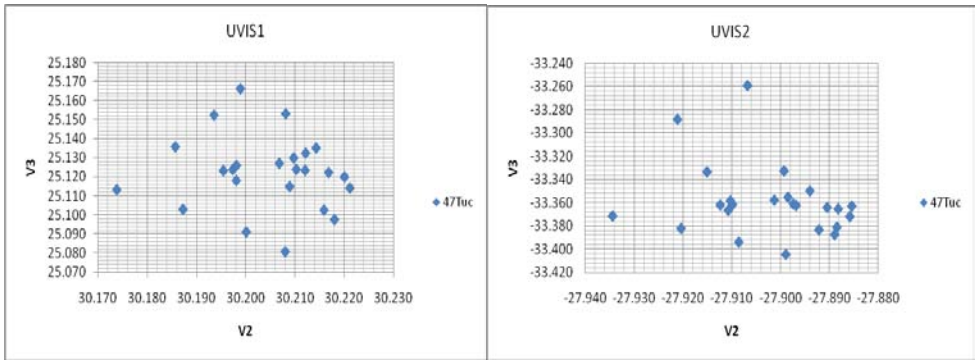

Figure 3 – (V2,V3) zero points for the distortion solutions of the individual 47 Tuc observations

Following this 'rediscovery' of the guider drift, it was decided that the best way to allow for this would be to take the average of the distortion coefficients (see Table 2) that are solved independantly for each observation, as in the (X,Y) method, and to adopt the more accurate (V2,V3) zero points from the WFC3-FGS alignment data.

The IR observations were analysed in the same way as the UVIS, however it should be noted that the number of stars in each field is lower due to both the small field of view and the location off center of the cluster. Typical errors for the distortion fit to each chip are 10-15 mas, and no systematic errors were found as a function of chip position or reference star magnitude. In figure 4, we show residuals for a typical individual obervation, the combined set for 47 Tuc and the (V2,V3) zero point drift which is spreading out the combined data residuals. Once again the mean distortion coefficients are listed in table 2.

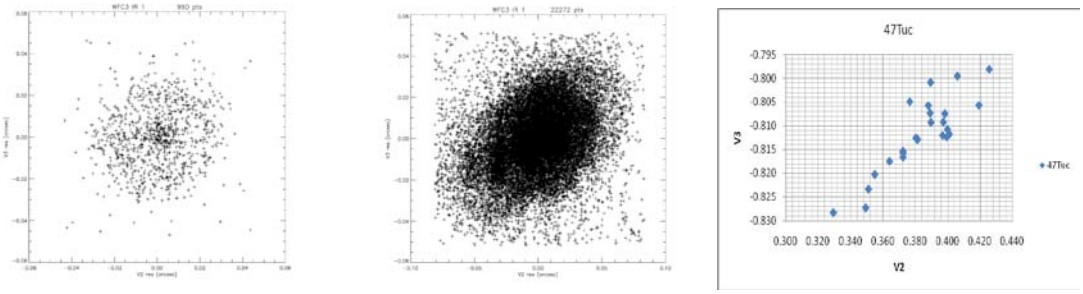

Figure 4 – (V2,V3) residuals between the reference catalog and the distortion solutions in a typical IR exposure in 47 Tuc, the residuals for the combined data and the (V2,V3) zero point drift

Table 2 - Average WFC3 Distortion Coefficients and their errors

[(x,y) pixels to (V2,V3) arcsec]

V2(x,y)	UVIS1	UVIS2	IR	V3(x,y)	UVIS1	UVIS2	IR
	+2.77484E-02	+2.80524E-02	+8.49871E-02		+2.79203E-02	+2.82878E-02	+8.60514E-02
a_{10}	(1.85455E-07)	(4.06116E-07)	(2.31167E-06)	b_{10}	(2.80909E-07)	(3.46281E-07)	(3.38667E-06)
	-2.61451E-02	-2.64854E-02	-9.60616E-02		+2.97916E-02	+2.97869E-02	+9.54570E-02
a_{11}	(2.29091E-07)	(2.98347E-07)	(4.53927E-06)	b_{11}	(1.87273E-07)	(2.80248E-07)	(3.53792E-06)
	-8.22947E-08	-9.07237E-08	+2.57430E-06		-8.32898E-08	-8.54920E-08	+2.61512E-06
a_{20}	(5.68034E-10)	(7.91880E-10)	(1.75153E-08)	b_{20}	(7.69723E-10)	(7.90573E-10)	(1.82816E-08)
	+1.55418E-07	+1.59281E-07	-2.37901E-06		-8.12652E-09	-8.93227E-09	+2.32220E-06
a_{21}	(1.98250E-10)	(4.40223E-10)	(1.89007E-08)	b_{21}	(2.58994E-10)	(4.66277E-10)	(1.66735E-08)
	-7.54107E-08	-7.84630E-08	+6.16081E-07		+8.48816E-08	+8.49905E-08	+5.93081E-07
a_{22}	(1.38681E-10)	(1.89719E-10)	(1.85053E-08)	b_{22}	(1.54715E-10)	(2.52237E-10)	(2.53244E-08)
	+5.76529E-13	-3.28880E-13	-7.85359E-12		+1.06437E-12	+1.13302E-12	-5.05952E-12
a_{30}	(3.50540E-13)	(5.82192E-13)	(1.41835E-11)	b_{30}	(3.65658E-13)	(4.32694E-13)	(1.38437E-11)
	-6.63381E-13	-4.72997E-13	-1.87655E-12		+2.85609E-13	+5.65713E-14	+3.92825E-12
a_{31}	(1.67651E-13)	(2.79179E-13)	(1.76632E-11)	b_{31}	(1.85881E-13)	(1.94627E-13)	(2.07041E-11)
	-2.24014E-13	+6.20263E-13	-3.32942E-11		+3.64169E-14	-2.42744E-14	-3.90086E-12
a_{32}	(6.15238E-14)	(8.94912E-14)	(1.63789E-11)	b_{32}	(7.24402E-14)	(1.41556E-13)	(1.56316E-11)
	+3.07740E-13	-4.68356E-13	+6.57604E-12		+6.74953E-13	+5.46615E-13	-1.73796E-11
a_{33}	(5.18914E-14)	(7.08628E-14)	(2.10866E-11)	b_{33}	(4.40902E-14)	(5.88596E-14)	(1.95898E-11)
	-2.82466E-16	+1.41875E-15	+6.56139E-14		+9.37182E-16	+2.36576E-17	+3.37313E-14
a_{40}	(6.26878E-16)	(7.36153E-16)	(6.93722E-14)	b_{40}	(7.63274E-16)	(7.89062E-16)	(8.55427E-14)
	-4.32512E-16	-4.36448E-16	-8.85841E-14		+5.40443E-16	-6.10576E-16	+6.63058E-14
a_{41}	(2.57820E-16)	(4.04854E-16)	(6.96661E-14)	b_{41}	(4.36837E-16)	(4.78837E-16)	(6.74684E-14)
	-1.20087E-17	+1.07886E-15	+2.26421E-14		+3.32233E-17	-2.79699E-17	-8.89411E-15
a_{42}	(1.37051E-16)	(3.55859E-16)	(6.06065E-14)	b_{42}	(1.42765E-16)	(2.29000E-16)	(6.68083E-14)
	-2.03173E-16	-2.39266E-16	-5.15501E-14		-2.68578E-18	+2.49404E-16	+1.16707E-13
a_{43}	(5.88532E-17)	(1.19265E-16)	(8.90755E-14)	b_{43}	(6.26194E-17)	(1.34084E-16)	(8.14905E-14)
	-1.71295E-16	+2.00223E-17	+1.10115E-14		+9.32813E-17	+7.91403E-17	-5.76122E-14
a_{44}	(4.42495E-17)	(6.33178E-17)	(7.02307E-14)	b_{44}	(4.04404E-17)	(6.78532E-17)	(1.05143E-13)

Comparison of Distortion Solution Methods

It should be noted here that it is not possible to directly compare these distortion coefficients to those computed by the (X,Y) method since they use different units and reference frames. In order to begin a comparison, it is first necessary to transform these into the (IDCTAB) form used by the ground-system reference files and by MultiDrizzle. The calibrations were derived in the 'natural' frame defined by the observation itself, but the reference frame used by the calibration software maintains the orientation of the Y axis at a fixed angle relative to the telescope coordinate system -V3 axis. This angle was chosen to be 45^o since it is close to the actual orientation of the instrument in the HST focal plane. The coeeficients can be rotated to this angle using the transformation described by

$$A_{ij} = -a_{ij}.\cos(45^o) + b_{ij}.\sin(45^o)$$
$$B_{ij} = a_{ij}.\sin(45^o) + b_{ij}.\cos(45^o)$$

and provides us with the IDCTAB coefficients for the (V2,V3) technique. One can also compute the scales and angles for both the X and Y axes as decribed in section 4 of the main text. If ones compares these to the values derived by the (X,Y) method, it can be seen that the scales agree but there is a small (but significant) rotation of the β angles.

Table 3 - Derived Parameters of Geometric Distortion

Parameter	UVIS1	UVIS2	IR
X_{scale}	0.03963 "/pix	0.03985 "/pix	0.1354 "/pix
Y_{scale}	0.03936 "/pix	0.03984 "/pix	0.1209 "/pix
β_X	-41.270 ^{o}	-41.642 ^{o}	-45.181 ^{o}
β_Y	+44.823 ^{o}	+44.761 ^{o}	+44.644 ^{o}

It must be emphasized that the distortion coefficients derived by this method provide the transformation for the *actual* aperture locations and geometry rather than those used by the preflight estimates. This is the reason for the small rotation of the β angles between the two methods. Since the ORIENTAT keyword and WCS information for each chip that is available in the image headers is populated using the SIAF (Science Instrument Aperture File) when the HST schedule is constructed, all of these calibration images will have the preflight geometry embedded in the values of these keywords. When MultiDrizzle is used, it will distort the images according to the coefficients in the IDCTAB and then shift and rotate the *existing* WCS by the aperture geometry also specified the IDCTAB. The (X,Y) technique creates an IDCTAB by using the ORIENTAT already in the headers so it is internally self-consistent and MultiDrizzle produces correctly aligned images. If we use the actual geometry that the (V2,V3) method determines, then we expect that using MultiDrizzle will result in a small rotation of the images because of the difference between the preflight and actual aperture geometry. An example plot of reference catalog residuals determined from a multi-drizzled frame is shown in figure 5. The significance of this is that when the SIAF changes, a corresponding change MUST be made to the IDCTAB. For any given observation, therefore, the IDCTAB must match the SIAF used when the SMS was generated.

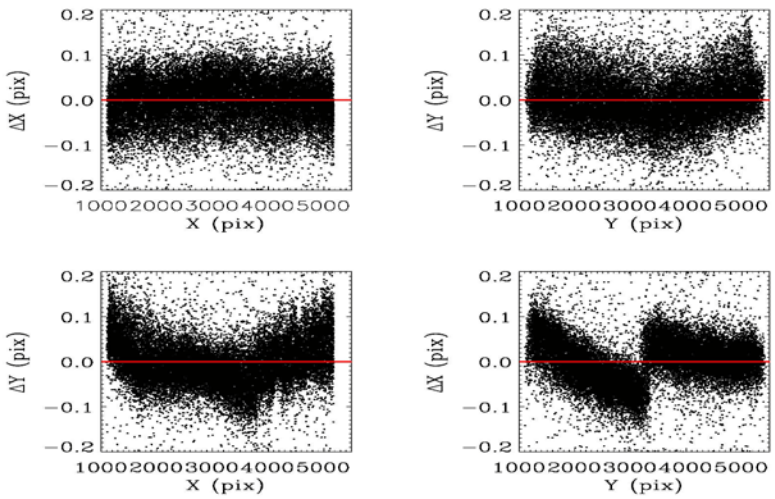

Figure 5 - typical UVIS residuals between the actual and observed locations of reference stars after MultiDrizzle for the (V2,V3) method IDCTAB due to the differences in the preflight geometry in the WCS and the actual derived geometry.

A quick illustration of this is take a grid of points across the chips, apply the two different IDCTABs and plot the differences between them. As can be seen in figure 6, the differences are predominantly a rotation of each chip.

In order to check our understanding of the interaction between the SIAF geometry, image header keywords, IDCTAB coefficients and MultiDrizzle we can take the (V2,V3) IDCTAB coefficients and rotate them by the β_Y angle difference so they should correspond to the (X,Y) method coefficients. If we then run MultiDrizzle and look at the residuals of the reference stars in the drizzled image we now find that the two techniques produce similar results since this now matches the preflight geometry embedded in the image keyword values (see figure 7).

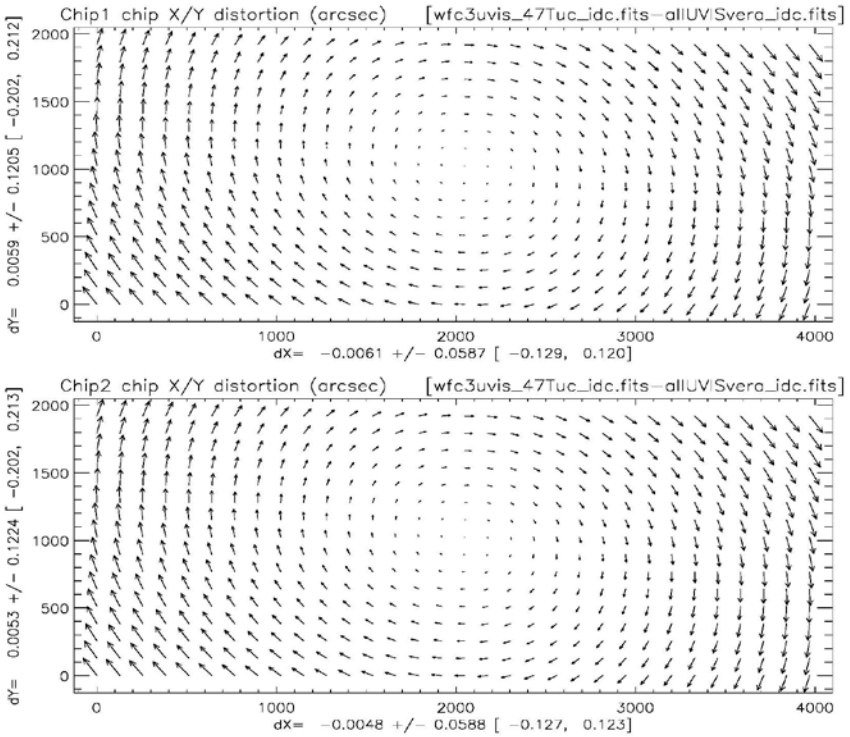

Figure 6a- Differences between the IDCTABs for the (V2,V3) and (X,Y) methods for the UVIS channel

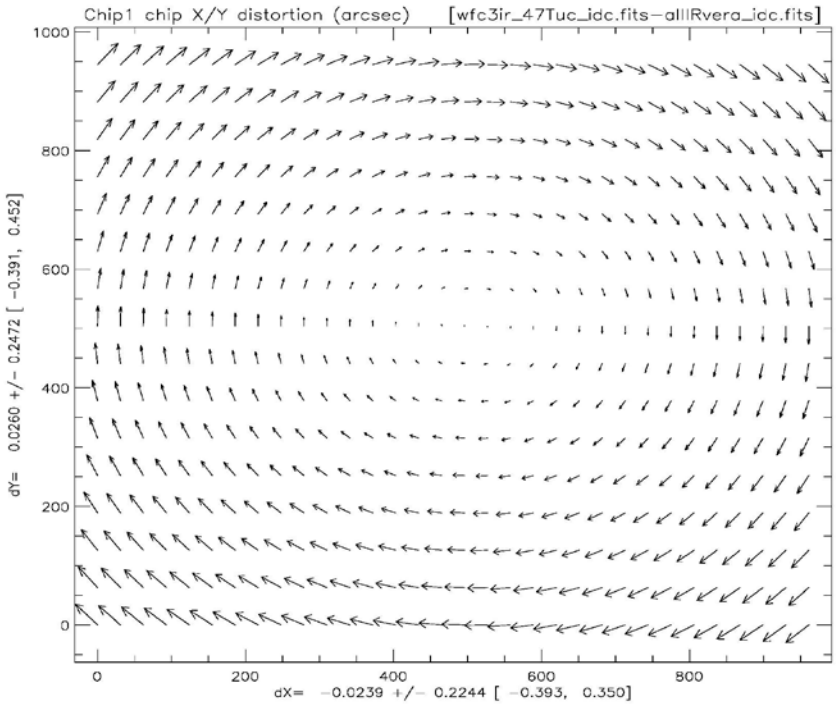

Figure 6b- Differences between the IDCTABs for the (V2,V3) and (X,Y) methods for the IR channel

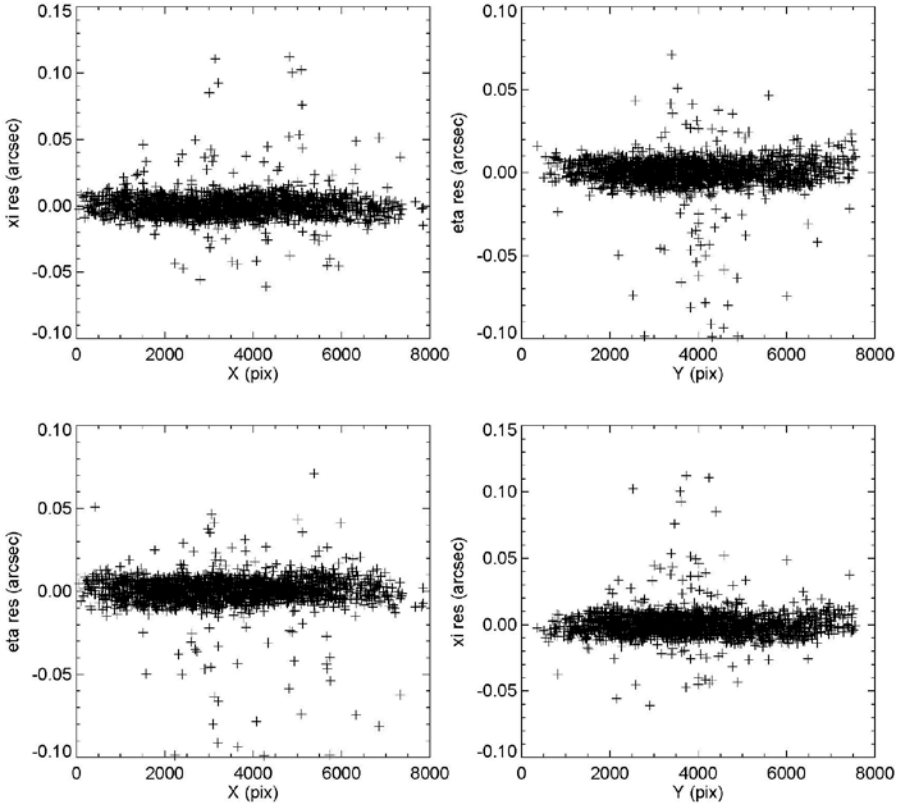

Figure 7 -typical UVIS residuals between the actual and observed locations of reference stars after MultiDrizzle using the (V2,V3) method IDCTAB after rotating to match the pre-flight SIAF geometry.

Comparison of UVIS Chip Separation

The other comparison that can be made between the IDCTABs for the two methods is to compute the locations of the chip edges and derive the chip separation for the UVIS detector. We find that for the UVIS channel the CCD chip gap runs from 30.00 pixels at one end of the detector to 32.35 pixels at the other end, which agrees with the derived values for chip separation and opening angle from the (X,Y) technique.

Comparison of Distortion Solutions with FGS Alignment Data

There were independant calibration proposals (11442 & 11443) to observe a field in the cluster NGC188 for which there is a highly accurate astrometric catalog that is used for both targets AND guide stars. This field is used for all science instrument aperture measurements. The positions of a number of stars in this field were measured to determine the absolute alignment of the WFC3 with respect to the FGS and hence its location in the HST focal plane. This is more fully described in ISRs by Dressel, Cox &

Lallo (2009a,b). These same X,Y measurements can be used with the derived distortion solutions to predict their V2,V3 coordinates which can be compared with their position based purely on the FGS measurements for that observation.

The solutions for both the (X,Y) and (V2,V3) methods were used to compare their predicted coordinates with the results from the Payload Operations Control Center (POCC) Applications Software Support (PASS) system. We find that the measurements corresponding to each individual star 'clump' together. This is because the measurement and distortion solution errors combined are smaller than the catalog errors between stars. The results for the (V2,V3) method are shown in figures 8a,b and show a good agreement to the FGS positions. The (X,Y) results are published in a separate TIR (Kozhurina-Platais et al (2009c).

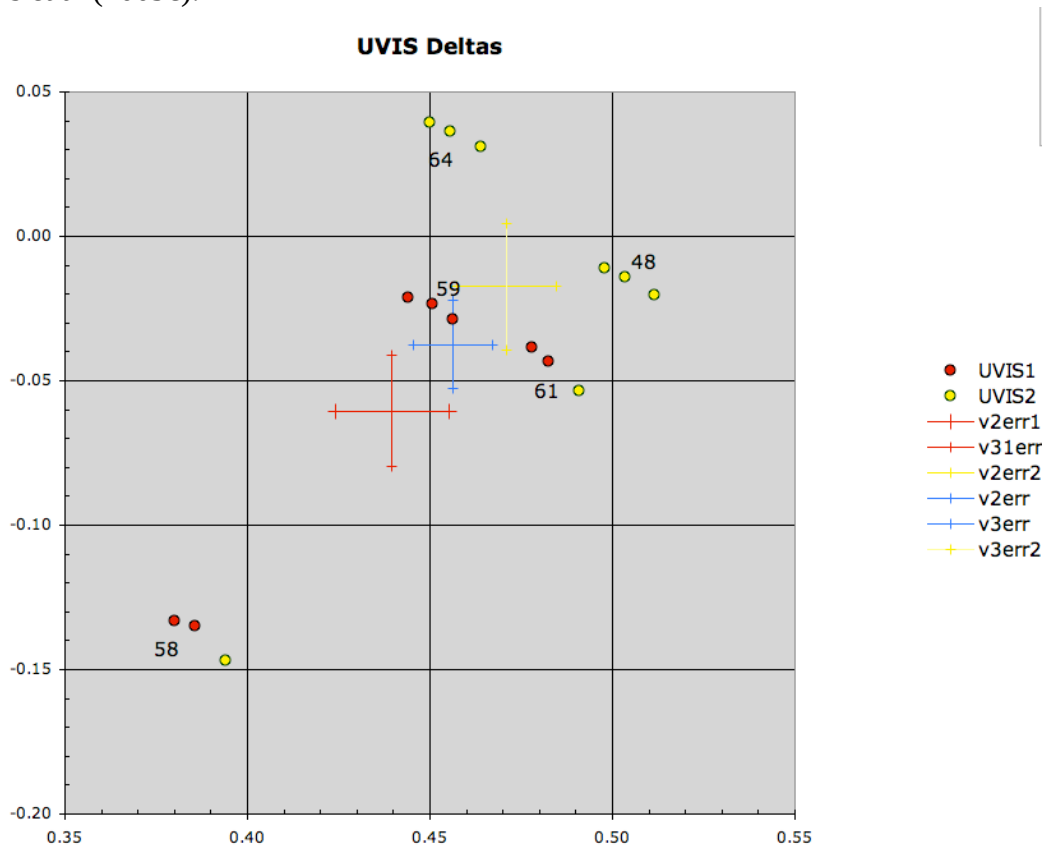

Figure 8a -Predicted (V2,V3) positions for NGC188 reference stars using IDCTAB from the (V2,V3) method for the UVIS channel.

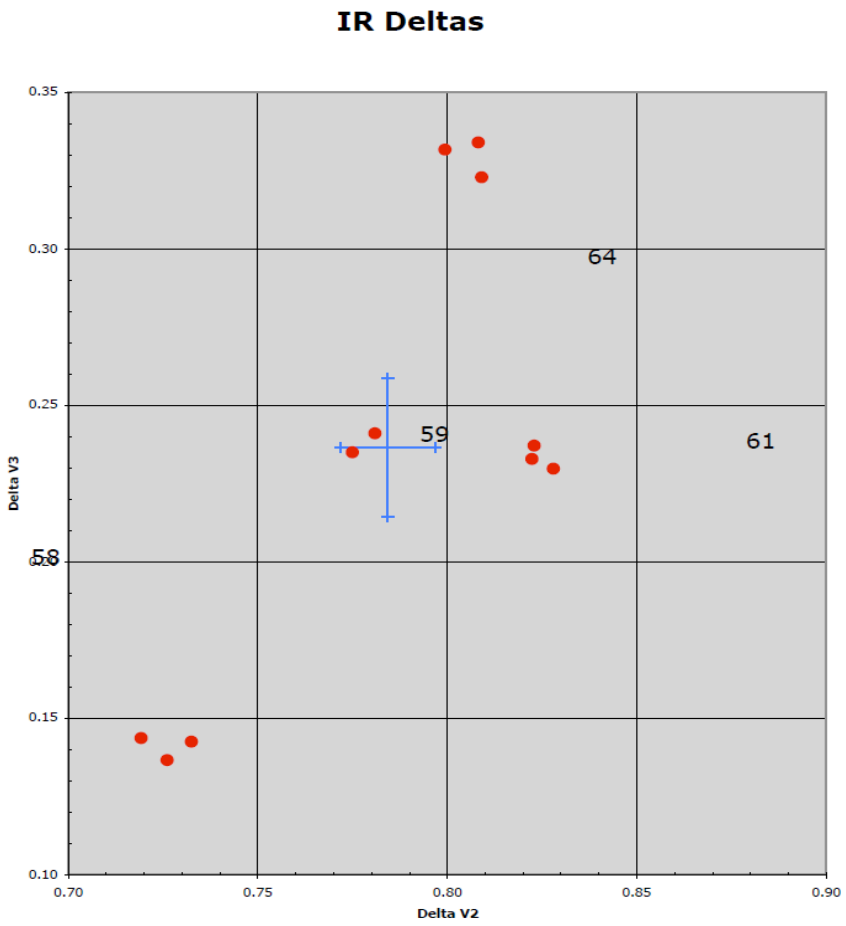

Figure 8b -Predicted (V2,V3) positions for NGC188 reference stars using IDCTAB from the (V2,V3) method for the IR channel.

As another check, the difference between the rotated (X,Y) IDCTAB and the (V2,V3) IDCTAB was computed and shown in figure 9. The size of the residuals is now reduced by a factor of 10x and the remaining small 'rotation' (0.02^{o}) is within the errors of the PASS results which have an estimated error of 0.04^{o}.

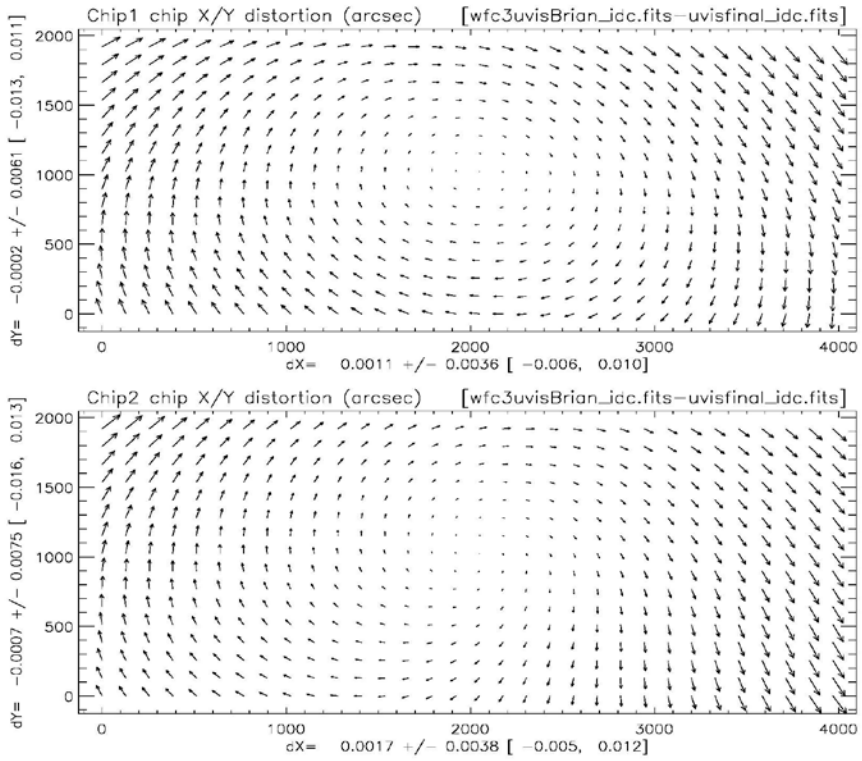

Figure 9a- Differences between the IDCTABs for the (V2,V3) and rotated (X,Y) methods for the UVIS channel. These difference are an order of mangitude smaller than the comparison to the unrotated (X,Y) IDCTAB.

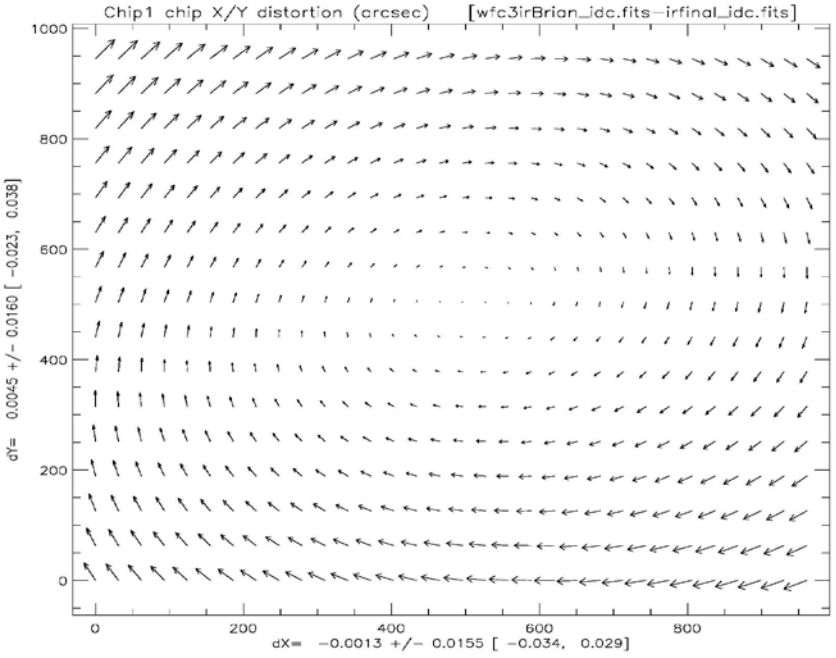

Figure 9b- Differences between the IDCTABs for the (V2,V3) and rotated (X,Y) methods for the IR channel. These difference are an order of mangitude smaller than the comparison to the unrotated (X,Y) IDCTAB.

Conclusions

These results confirm that the optical distortion of the WFC3 instrument has been modelled to of order 0.1 pixels by 2 independant methods, however, it does highlight the interdependance of the SIAF, IDCTABs and MultiDrizzle software.

Recommendations

It should be noted that it is necessary to synchronize updates to the IDCTAB and SIAF, at least when significant changes to angles are noted. The SIAF contents feed into the science data headers and subsequently affect the drizzle products. Both calibration files contain date stamps indicating the starting time when they are applicable, so this coordination can be arranged even though actual delivery dates may be different.

References

Dressel, Cox & Lallo (2009a) - Instrument Science Report WFC3 2009-35: Alignment of thd WFC3/UVIS Apertures to the FGS Coordinate Frame

Dressel, Cox & Lallo (2009b) - Instrument Science Report WFC3 2009-36: Alignment of thd WFC3/IR Apertures to the FGS Coordinate Frame

Gilliland (2005) - Instrument Science Report TEL 2005-02 Guiding Errors in 3-Gyro: Experience from WF/PC, WFPC2, STIS, NICMOS and ACS

Kozhurina-Platais, Cox, McLean, Petro, Dressel, Bushouse and Sabbi (2009a) - Instrument Science Report WFC3 2009-33 WFC3/UVIS Geometry Distortion Calibration

Kozhurina-Platais, Cox, McLean, Petro, Dressel, Bushouse and Sabbi (2009b) - Instrument Science Report WFC3 2009-34 WFC3/IR Geometry Distortion Calibration

Kozhurina-Platais et al (2009c) - Technical Instrument Report 2010-xxx In preparation

Lasker et al (2008) -The Second Generation Guide Star Catalog : Description and Properties 2008 A.J. 136,735